Growth and structure of pentacene films on graphite: Weak adhesion as a key for epitaxial film growth

Jan Götzen,[1] Daniel Käfer,[2] Christof Wöll,[3] and Gregor Witte[1,*]

[1]*Molekulare Festkörperphysik, Philipps-Universität Marburg, D-35032 Marburg, Germany*
[2]*Physikalische Chemie I, Ruhr-Universität Bochum, D-44780 Bochum, Germany*
[3]*Institut für Funktionelle Grenzflächen, Karlsruhe Institute of Technology, D-76021 Karlsruhe, Germany*

The microstructure of pentacene films grown on the basal plane of graphite has been investigated. By combining various complementary techniques including scanning tunneling microscopy, atomic force microscopy, x-ray diffraction, thermal desorption spectroscopy, and x-ray absorption spectroscopy the molecular orientation, crystalline structure, and morphology of the films as well as their thermal stability have been characterized in detail as a function of the film thickness. Initial film growth leads to the formation of a commensurate monolayer consisting of flat-lying molecules while upon subsequent deposition epitaxially ordered (022)-oriented pentacene films are formed which adopt the Siegrist phase. The detailed analysis shows that this epitaxial growth of films with an essentially recumbent molecular orientation is brought about by a slight rotation of the molecules in the first layer around their long molecular axis upon deposition of overlying molecular layers. Such a structural modification is unusual and becomes possible by the rather weak adsorption energy on graphite. In contrast, a very different film structure including an upright orientation of molecules even in the first layer is found on nonperfect but rough graphite surfaces leading to the formation of (001)-oriented films which initially reveal the thin-film phase and continue to grow in the Campbell phase of pentacene.

PACS number(s): 61.66.Hq, 61.30.Hn, 68.43.−h, 68.55.−a

I. INTRODUCTION

The promising perspective of using organic semiconductors to assemble thin film electronic devices[1–5] has aroused significant interest in a fundamental understanding of the microstructure and growth properties of such molecular films.[6,7] A specific peculiarity of these materials is the shape anisotropy of the molecular entities which causes a pronounced directional ordering and packing in the crystalline phase[8] and commonly leads to a pronounced anisotropy of the charge transport along the various crystallographic directions.[9,10] Therefore, a precise control of the molecular packing and crystalline orientation of thin films is of vital interest for an optimization of thin film devices. Since in the initial stage of film formation the molecular arrangement is largely governed by the interplay of intermolecular and molecule-substrate interactions one approach to control the molecular orientation and film structure is based on substrate mediated growth.[11–16]

Pentacene ($C_{22}H_{14}$) constitutes one of the most outstanding organic semiconductors allowing, e.g., the fabrication of well-performing thin film transistors[17,18] and has become a prototypical system of organic film growth which is widespread studied.[19] Deposition on inert substrates such as SiO_2, alkali halides or polymers favors an upright molecular orientation and the formation of polycrystalline films with (001) texture.[20–25] In case of KCl and Bi(0001)/Si the molecular and substrate lattice reveal a close match leading even to an epitaxial orientation of the pentacene films.[26–28] In contrast, on single-crystalline metals pentacene initially forms a chemisorbed monolayer of flat lying molecules while in subsequent layers the molecules arrange in a tilted fashion and the films reveal a pronounced islanding.[14–16,29–32] The under-

lying dewetting has been related to a strain release caused by the large lattice mismatch between the densely packed molecules in the chemisorbed monolayer and the packing motifs adopted in any molecular plane of the crystalline lattice of pentacene.[6]

Graphite is a particular interesting substrate for the growth of polycyclic aromatic hydrocarbons (PAHs) because on one hand it is chemically rather inert hence avoiding strongly bound molecules at the interface while on the other hand the carbon lattice of the basal plane of graphite is almost identical to the carbon frame of the molecular aromatic rings which may favor an epitaxial ordering at the interface. Moreover, in connection with the exceptional electronic properties of graphene[33] the modification of the electric transport in such material by the adsorption of molecules has become a topic of recent interest.[34,35]

Well-ordered basal planes of graphite can be easily prepared by exfoliation of highly oriented pyrolytic graphite (HOPG) which provides a convenient method to prepare atomically flat surfaces. In fact, the formation of well-ordered monolayer films has been observed for various planar PAHs adsorbed on graphite.[36–46] While this ordered films may serve as nucleation layer for further growth of ordered films the evolution of subsequent multilayers has yet not been studied systematically.

Using Penning-ionization spectroscopy Harada *et al.* have demonstrated already in 1984 that pentacene molecules adsorb on graphite in a planar adsorption geometry at low coverage while they become gradually tilted in subsequent layers with increasing coverage.[47] Regarding the crystalline structure of such multilayer films a polymorphism was previously reported which exhibits a characteristic molecular interlayer distance of 3.7 Å thus indicating weakly tilted or

recumbent orientated molecules.[48] In contrast to that high resolution scanning tunneling microscopy (STM) data reveal a reorientational growth from planar oriented pentacene in the first monolayer on HOPG to upright orientated molecules in multilayers forming (001)-oriented films[49] like on Bi(0001). Using temperature dependent photoemission electron microscopy (PEEM) measurements the preparation of a distinct pentacene monolayer on HOPG has been reported. This procedure is based on selective sublimation of multilayers upon annealing at 375 K and results in a residual monolayer[50] which was utilized to characterize the hole-vibration coupling in pentacene layers on graphite.[51] This finding about the thermal stability of pentacene films is somewhat surprising, since previous thermal desorption spectroscopy (TDS) measurements of various extended PAHs such as coronene and ovalene on HOPG yielded no distinct monolayer peak as it was observed for the smaller acenes benzene and naphthalene,[52] hence indicating the absence of a particularly stabilized monolayer which parallels the situation of pentacene on SiO_2.[32] Unfortunately, at present no TDS data are available for the system pentacene/HOPG which would allow for a direct determination of the adsorption energies of monolayer and multilayers of pentacene on graphite.

To resolve some of the apparent inconsistencies between the different reports on the growth of pentacene on graphite and to derive a more detailed understanding of the film formation of PAHs on graphite we have carried out a comprehensive study on the structure, stability, and evolution of pentacene layers on HOPG. This system can be considered as prototypical for organic film growth on weakly interacting but well-defined substrates which further may serve as a benchmark system for a theoretical analysis of van der Waals bound molecules at surfaces.[53] By combining various microscopy, diffraction and spectroscopic techniques including STM, atomic force microscopy (AFM), x-ray diffraction (XRD), TDS, and x-ray absorption spectroscopy (NEXAFS) we were able to derive a rather detailed picture of the structure and evolution of monolayer and multilayer films of pentacene on HOPG.

II. EXPERIMENTAL SECTION

All films were grown onto ZYA grade HOPG substrates (SPI supplies, mosaicity $<0.4°$) which in each case were cleaved in air using adhesive tape before loading into the ultrahigh vacuum (UHV) chamber. Particular care was taken to avoid graphite flakes sticking out of the surface, because such regions affect the XRD and NEXAFS measurements, by compressing both sides after cleavage and afterwards sliding them laterally apart. The substrates were mounted onto sample holders either by conductive tape (Plano) or by metal clips which also enable sample heating prior to deposition. All pentacene (Aldrich, purity $>99\%$) films were deposited under UHV conditions from a glass crucible of a resistively heated Knudsen cell at typical deposition rates of $5-10$ Å/min as determined by a quartz crystal microbalance.

The resulting films were characterized *in situ* using differ-ent UHV instruments. The initial stage of film growth and the molecular ordering in the (sub)monolayer regime were characterized by a scanning tunneling microscope (Jeol JSPM-4500S) which can also be operated at low temperatures of 80 K. All STM measurements were performed in constant current mode (typical values $I=30$ pA) using freshly etched tungsten tips.

Thermal desorption experiments were conducted in a separate instrument employing a quadrupole mass spectrometer (Balzers QMA 200) with a Feulner cup positioned close to the sample surface. TD spectra were measured by recording two mass signals (M^+ and M^{++}, $E_{ion}=85$ eV) during a computer-controlled linear increase of the substrate temperature from 290 to 800 K with a heating rate of $\beta=0.5$ K/s. The temperature was measured by a K-type thermocouple attached directly to the surface. Typically seven spectra were acquired for signal averaging and to verify the reproducibility of the individual runs.

The NEXAFS measurements were performed in a third UHV instrument at the synchrotron storage ring BESSY II in Berlin (Germany) at the dipole beamline HE-SGM applying linear polarized synchrotron light with a polarization factor of $P \approx 85\%$. All NEXAFS measurements were recorded with an energy resolution of about 100 meV at the C K edge in partial electron yield mode using a channel plate electron detector with a retarding field of -150 V. For energy calibration the photocurrent of a carbon contaminated gold grid in the incident beam was recorded simultaneously with each spectrum yielding a characteristic absorption peak at 284.90 eV which had been cross-calibrated by clean graphite. The NEXAFS raw data have been evaluated in a multistep procedure comprising an energy calibration, a flux normalization by dividing the spectra by corresponding data of a clean gold sample serving as reference substrate to account for the transmission,[54,55] and finally an edge jump normalization.

These data were completed by *ex situ* measurements of the morphology and crystallography of the pentacene films. Tapping mode AFM (Jeol JSPM 4210) was used to characterize the film morphology while the crystallographic phase and orientation of the films were determined from XRD data acquired with a diffractometer (Bruker, D8 Advance) operated in Bragg-Brentano geometry using Cu $K\alpha_1$ radiation ($\lambda=1.54051$ Å) and a position sensitive detector.

III. RESULTS

A. Thermal stability

Previous studies reported the possibility of preparing a distinct pentacene monolayer on HOPG by heating afore grown multilayer films at 375–380 K for several hours in order to thermally desorb the multilayer excess.[50,51] A similar approach was utilized in earlier studies to produce a well-defined monolayer of pentacene on various metal substrates such as Cu, Ag, and Au.[15,31,32] To characterize the thermal stability of the films and to figure out a useful temperature range for the post-deposition thermal treatment, at first TDS measurements were carried out. To enable a removal of potential contaminations the samples were first heated at 700 K for several hours in vacuum prior to film deposition. Figure 1
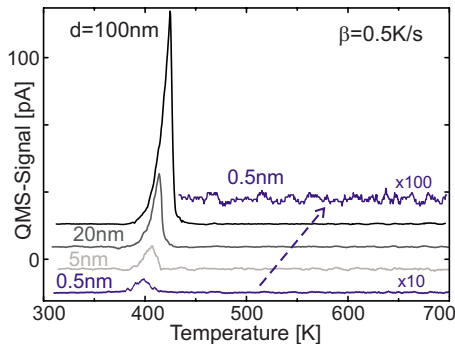
FIG. 1. (Color online) Series of thermal desorption spectra of pentacene films on HOPG recorded for different film thicknesses at the mass of the molecular ion ($m/z=278$ amu).

displays a typical series of TD spectra recorded for pentacene layers of different thickness grown at room temperature onto HOPG. All spectra exhibit only one distinct desorption peak around 400–425 K. While the onset of all peaks remains constant at about 385 K their intensity, peak area, and maximum increase with film thickness and thus can be assigned to multilayer desorption. In fact, a detailed analysis shows that the desorption peak is well described by zero-order kinetics. Using an Arrhenius ansatz the ascending peak flank is well described by $\ln I \sim E_{des}/RT$ as expected for multilayer desorption. A fit to the experimental data (so-called *leading edge analysis*)[56] yields an activation energy for desorption of 152.2 kJ/mol (1.58 eV). This value is in close agreement with the standard sublimation enthalpy of pentacene of $H_{sub}=156.9$ kJ/mol (Ref. [57]) which equals the adsorption energy in case of a nondissociative adsorption without barriers. No further desorption peak even at the mass of characteristic fragments could be detected at higher temperatures hence indicating the absence of a firmly bound first monolayer. Interestingly, also the desorption signal from a (sub)monolayer film (thickness 0.5 nm) fits to the ascending flank of the multilayer desorption peaks suggesting a dewetting and formation of multilayer islands upon heating. The present system thus parallels the situation observed for pentacene on SiO_2 (Ref. [32]) where in contrast to pentacene adsorption on metals no specific monolayer can be prepared by heating.

B. Monolayer structure

Based on the results described in the previous section we have grown (sub)monolayer films with a nominal thickness of 0.3–0.5 nm in order to suppress multilayer formation and to enable a structural characterization of the first monolayer. Figure 2(a) displays a typical large area STM micrograph revealing the presence of elongated, straight islands. The height distribution analysis [see Fig. 2(c)] confirms the absence of multilayers and yields a monolayer height of 2.2 Å. Note, that this value is in close agreement with the effective *thickness* of pentacene by considering the van der Waals dimensions (15.6 Å × 6.4 Å × 2.4 Å) obtained from a density-functional theory (DFT) calculation using a 98% electron density contour,[30] hence reflecting a planar adsorp-
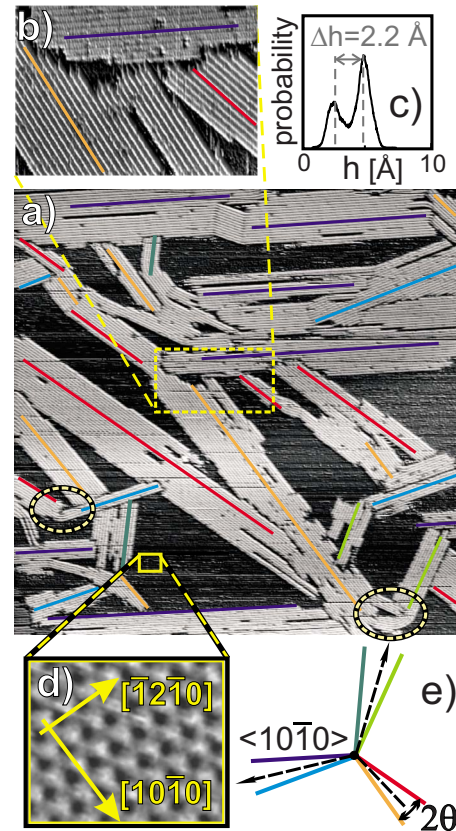

FIG. 2. (Color online) Room-temperature STM data of sub-monolayer pentacene films grown on HOPG. (a) Large area scan (315 nm × 315 nm, $U_{sample}=-2.0$ V, I=30 pA) together with (b) magnified image revealing a characteristic row pattern on the islands and (c) corresponding height distribution. Panel (d) shows an STM micrograph ($U_{sample}=0.6$ V, I=0.5 nA) of the atomic lattice of the bare HOPG-surface between the islands which yields (e) a discrete orientation of the row patterns relative to the substrate $\langle 10\bar{1}0 \rangle$ azimuth directions (dashed lines).

tion geometry with the molecular plane parallel to the surface. This adsorption geometry is in line with earlier findings.[47,58]

A closer view [see magnified image in Fig. 2(b)] reveals furthermore the presence of closely spaced rows on the individual islands that are aligned parallel to the long edges of the islands. A systematic analysis of the orientation of all row patterns on areas which can be considered as single crystalline domains of graphite (typically several μm) allows further a determination of the angular distribution of the islands. This yields 6 distinct azimuthal orientations appearing as three pairs rotated by 120° relative to each other and a splitting of $2\theta \approx 18° \pm 3°$ of each pair [indicated by colored lines in Figs. 2(a) and 2(e)]. Additional information about the orientation relative to the substrate was obtained by also imaging the substrate lattice. Since it was not possible to acquire simultaneously high-resolution data of the film and the substrate subsequent images with different tunneling conditions but same scan direction were recorded to resolve the atomic lattice of the graphite substrate between the pentacene islands [see Fig. 2(d)]. The result of this analysis is displayed in Fig. 2(e) and reveals that each pair of similarly oriented
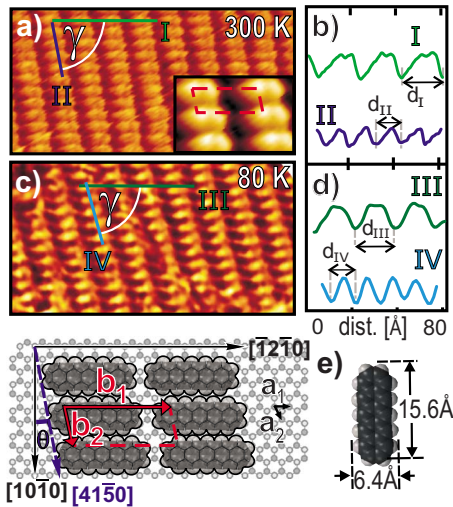
FIG. 3. (Color online) High-resolution STM data of the pentacene monolayer on HOPG with corresponding line scans recorded (a) and (b) at room temperature and (c) and (d) at 80 K (U_{sample} = −2.0 V, I = 30 pA). The inset in (a) reveals a correlated averaged image and panel (e) depicts a model of the identified monolayer structure and the van der Waals dimensions of pentacene.
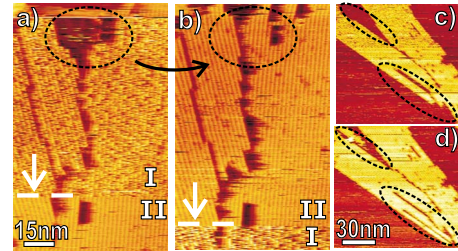

FIG. 4. (Color online) (a) and (c) Room temperature STM micrographs of two different regions of a pentacene submonolayer on HOPG (U_{sample} = −2.0 V, I = 30 pA). The consecutively recorded STM data (b) and (d) reveal characteristic morphological changes of the island shape (indicated by dashed loops) occurring on a time scale of minutes which reflects a weak binding to the substrate. Moreover, sudden tip switches [denoted as I and II in (a) and (b)] were frequently observed during initial stage of imaging and indicate the presence of mobile admolecules on the substrate due to weak adsorption.

islands is actually centered around the $\langle 10\bar{1}0 \rangle$ azimuth directions of the substrate.

Next, we have analyzed the molecular ordering within the monolayer islands. Figure 3(a) depicts a high resolution STM micrograph recorded at room temperature together with a correlated averaged image (inset) showing the arrangement of individual molecules. All molecules are uniformly aligned with their long axis along $\langle \bar{1}2\bar{1}0 \rangle$ directions and form an oblique unit cell with lateral dimensions of d_I = 17.2 ± 0.5 Å and d_{II} = 7.0 ± 0.5 Å forming an angle of γ = 78° ± 3°. Additional STM data which were acquired at 80 K [Figs. 3(c) and 3(d)] yielded almost identical unit cell parameters (d_{III} = 17.4 ± 0.5 Å and d_{IV} = 7.3 ± 0.5 Å forming an angle of γ = 76° ± 3°). By comparing these dimensions with the atomic lattice of the C(0001) surface the pentacene monolayer can be identified as a $\left(\begin{smallmatrix} 7 & 0 \\ -1 & 3 \end{smallmatrix} \right)$ superstructure with the unit cell vectors $\mathbf{b_1}$ = 17.22 Å and $\mathbf{b_2}$ = 6.51 Å drawing an angle of 79.1° which is shown schematically in Fig. 3(e). The commensurability of the pentacene monolayer which is favored by the close match of the molecular carbon frame and the substrate (C-C distance in pentacene varies from 1.35 Å in the outermost to 1.45 Å in the central ring and amounts to 1.42 Å in the basal plane of graphite) is supported by the appearance of discrete island orientations. A comparison of the length of the unit cell vector $\mathbf{b_1}$ with the van der Waals length of pentacene indicates further that the molecules are not densely packed along $\langle \bar{1}2\bar{1}0 \rangle$ directions. Instead, they reveal a small but noticeable gap between the head sides of neighboring molecules which is caused by the registry with the substrate and leads to the characteristic row pattern. Sideways a close packing is achieved by shifting adjacent molecules alongside one substrate unit which results in the distinct orientation of the apparent rows along the $[41\bar{5}0]$ azimuth forming an angle of θ = 10.9° with the $[10\bar{1}0]$ substrate direction.

Note, that despite the commensurability of the pentacene monolayer the molecules interact only weakly with the graphite surface which leads to some peculiarities. At regions where neighboring islands coalesce molecules form dense packed but bent connections [cf. dashed circle in Fig. 2(a)] which indicate a small corrugation of the substrate holding potential. Because of the weak adsorption of pentacene at the graphite substrate isolated admolecules are quite mobile and can easily attach/detach to/from existing islands leading to characteristic changes of island boundaries observed in consecutively recorded STM images as shown in Fig. 4 (dashed lines). The presence of mobile admolecules also causes sudden tip switches especially during first scans of regions [indicted by I and II in Figs. 4(a) and 4(b)] due to pick-up and release of molecules. These events occur also at 80 K hence indicating a large mobility even at low temperatures which is in line with the weak adsorption.

C. Morphology of multilayers

Since the low conductivity of molecular multilayers hampers the use of STM for a systematic structural analysis the film morphology was at first characterized by means of tapping mode AFM. Pentacene films with a thickness of a few nanometers consist of narrow, plank shaped, or laminar islands extending over several microns as depicted in Figs. 5(a) and 5(b). A detailed analysis shows that these islands are rather smooth and exhibit distinct steps of about 4 ± 1 Å which suggest a recumbent orientation of the molecules within such films. Note, that the substrate is not completely covered and reveals deep crevices between the individual islands of which height exceeds the nominal film thickness. With increasing film thickness the islands become larger and still persist ultraflat but remain disconnected [cf. Fig. 5(c)]. We note further, that no significant morphological changes were observed on pentacene films after heating them at about 360 K for 2 h in vacuum or keeping them several months at room temperature in air.

At some parts of the surface, however, a rather different film structure was found and discoid, pyramidal islands were
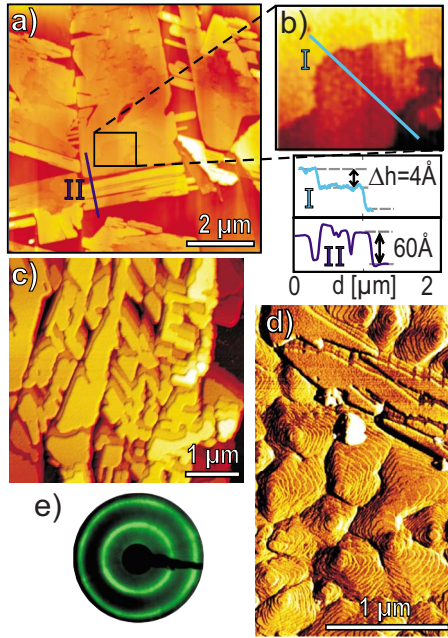
FIG. 5. (Color online) Room-temperature tapping mode AFM micrographs showing the morphology of pentacene films grown on HOPG (8 Å/min). (a) For a 3 nm film together with a magnification (b) and corresponding line scans revealing the island height and the presence of monomolecular steps and (c) for a nominal thickness of 35 nm. (d) AFM phase image representing the minority of film structures that were occasionally found on the same sample although the HOPG substrates were carefully prepared as evidenced by (e) LEED pattern (196 eV) of the bare graphite surface before the deposition.

observed [see Fig. 5(d)] which are similar to those obtained for pentacene films grown on SiO_2.[19] In fact the height analysis reveals distinct steps of about 15 Å which is in close agreement with the (001)-interlayer spacing in pentacene crystals and thus suggests a film structure of upright standing molecules. At this point we emphasize that this unusual morphology was found locally on several samples although the substrates had been carefully prepared and some samples had also been heated in vacuum at 700 K for several hours before deposition. To demonstrate the good ordering of the substrate a low-energy electron diffraction (LEED) pattern of the bare HOPG surface before pentacene deposition is shown in Fig. 5(e). The sharp ring pattern reflects a high local ordering which is azimuthally averaged on a large scale. This kind of ordering is characteristic for HOPG (Ref. 59) and hampers the use of LEED to identify the pentacene film structure. In a previous study we found that the morphology and growth of pentacene films on gold substrates depends critically on the surface roughness.[30] Therefore the appearance of the pyramidal islands on HOPG is tentatively attributed to inhomogeneities or disorder of the graphite surface. To scrutinize this hypothesis additional pentacene films were grown on HOPG that was briefly sputtered with Ar^+ ions (10 min, 700 eV) before deposition in order to create a rough surface. In fact, a rather different film structure is found on such defective substrates as shown in Fig. 6. Typical AFM micrographs reveal the presence of dendritic is-
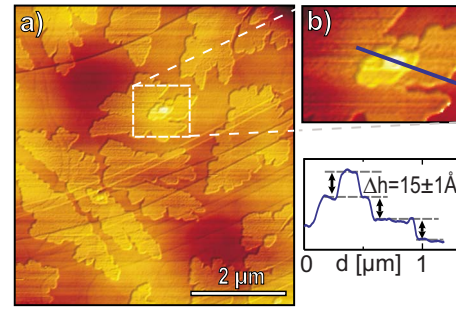

FIG. 6. (Color online) (a) Room-temperature AFM data of a 2 nm pentacene film grown onto briefly sputtered HOPG revealing dendritic islands. The line scan of the magnified image (b) yields a step height which indicates an upright orientation of the molecules.

lands with distinct steps of 15 Å which are in line with upright standing pentacene molecules like in the case of SiO_2 hence emphasizing the importance of the surface roughness on the resulting film structure.

D. X-ray diffraction

To identify the crystalline phases and orientation of the pentacene films they have been further analyzed by XRD measurements which are summarized in Figs. 7(a)–7(c). In case of thin films the characteristic (0002) reflex of the substrate at $2\theta = 26.61°$ (corresponding to a layer spacing of $d = 3.36$ Å) was used as an intrinsic reference to compensate possible angular offsets of the diffractometer.

Figure 7(a) displays a $\theta/2\theta$ scan of a 20 nm pentacene film which reveals in addition to the C(0002) peak two further reflexes, an intense one at 24.04° and a much weaker at 25.53°. Based on a comparison with powder diffraction patterns which were calculated[60] for the three known crystal structures of pentacene [Figs. 7(d)–7(f)] Siegrist phase,[8] Campbell phase,[61] and thin film phase[62,63] the two diffraction peaks can be clearly identified as (022) and $(1\bar{1}3)$ reflexes of
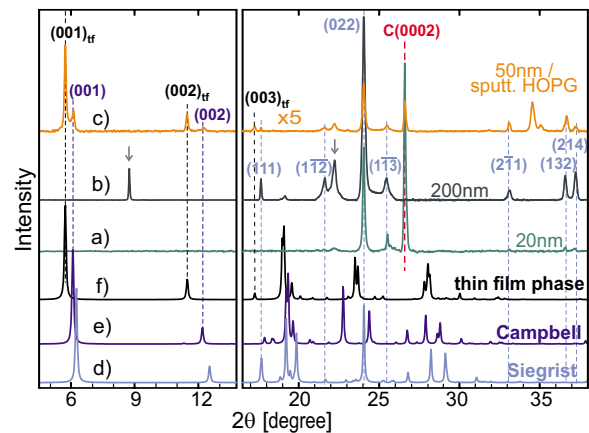

FIG. 7. (Color online) $\theta/2\theta$ scans of different pentacene films grown on HOPG: (a) 20 nm (5 Å/min, 300 K), (b) 200 nm (15 Å/min, 300 K), and (c) 50 nm (10 Å/min, 300 K) deposited on sputtered HOPG, together with the powder diffractograms calculated for the various crystalline phases of pentacene: (d) Siegrist phase, (e) Campbell phase, and (f) thin film phase.

the Siegrist phase with corresponding interplanar spacings of 3.70 Å and 3.49 Å, respectively. Note that the major peak has been observed before for a pentacene film on graphite,[48] but was assigned incorrectly to the (200) reflex of a putative new polymorphism.

For a 200 nm pentacene film the substrate related reflex is no longer visible but in addition to the still dominating (022) reflex several weaker peaks appear at 8.75° ($d = 10.10$ Å), 17.64° (5.02 Å), 19.13° (4.64 Å), 21.61° (4.11 Å), 22.22° (4.00 Å), 25.45° (3.50 Å), 33.12° (2.70 Å), 36.59° (2.45 Å), and 37.24° (2.41 Å). While the first and fifth of these peaks [indicated by arrows in Fig. 7(b)] cannot be assigned to one of the known crystallographic phases the other ones can be indexed as (111), (10$\bar{2}$), (1$\bar{1}$2), (1$\bar{1}$3), (2$\bar{1}$1), (132), and (214) reflexes of the Siegrist phase. The nonindexed peaks might be attributed to additional crystalline fibers which have been observed before on top of thick pentacene films[30] and exhibit a nonsubstrate related skeleton growth.

As already indicated by the AFM data a rather different film growth proceeds on rough graphite substrates which is further corroborated by the corresponding diffraction data. Figure 7(c) displays a diffraction pattern of a 50 nm pentacene film that was grown onto a HOPG surface which had been additionally sputtered (3 h, 1.2 keV Ar$^+$ ions) after cleavage. After this treatment the characteristic ring structure could no longer be observed in the corresponding LEED data thus indicating a substantial disorder. The x-ray diffractogram reveals intense reflexes at small angles of $2\theta = 5.74°$, 11.47°, and 17.25° which can be assigned to first and higher order Bragg peaks of the (001) plane of the thin film phase exhibiting an interplanar spacing of 15.4 Å. The additional much weaker replica at 6.10° and 12.25° arise from the (001) plane ($d = 14.4$ Å) of pentacene in the Campbell phase. At larger diffraction angles (16.5°–38°) some more but less intense peaks were observed which originate from crystalline pentacene adopting the Siegrist phase and presumably can be related to small islands formed on rather intact graphite areas. Apparently the high defect density on rough HOPG substrate favors an upright orientation of pentacene molecules and a subsequent growth of (001) oriented films which is thermodynamically most favorable.[64] The observed texture and orientation of pentacene films on rough graphite substrates thus parallels the situation occurring upon growth on SiO$_2$ and other inert substrates like KCl (Ref. 26) or PTFE (Ref. 21) where a transition from the initially formed thin film phase to the Campbell phase appears with increasing film thickness.[20,65]

In contrast, pentacene films deposited onto highly ordered and smooth graphite substrates crystallize in the Siegrist phase and thereby mainly form a (022)-contact plane. In this crystallographic plane the molecules are procumbent thus enabling a large contact area with the substrate.

E. NEXAFS

Additional information on the electronic coupling and orientational order of pentacene molecules in the various films were obtained from x-ray absorption spectroscopy. In con-
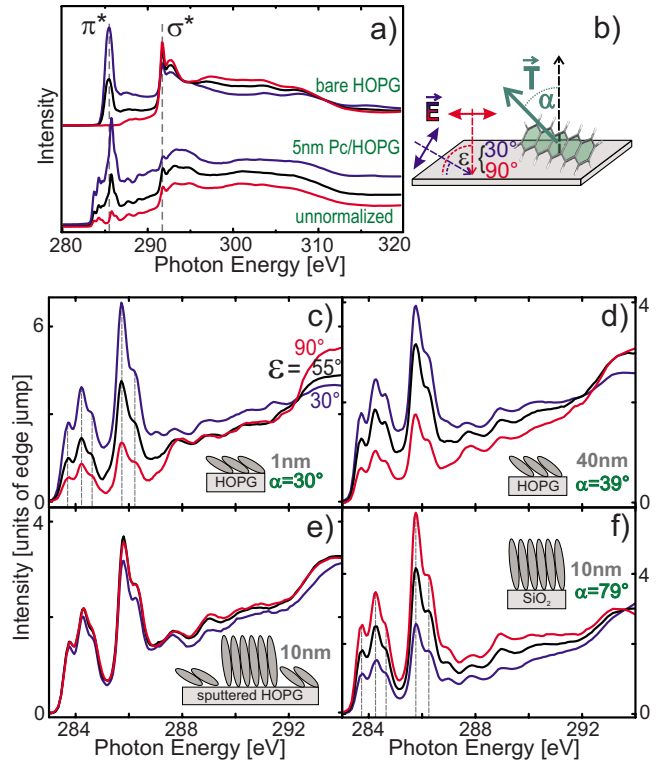

FIG. 8. (Color online) Series of C1s NEXAFS spectra recorded for bare and pentacene covered HOPG: (a) clean graphite substrate compared with un-normalized spectra of a 5 nm pentacene film on graphite (300 K, 10 Å/min). Panels (c)–(f) display the magnified π^* region of the NEXAFS spectra of differently prepared pentacene films: (c) 1.0 nm on HOPG (300 K, 2 Å/min), (d) 40 nm on HOPG (300 K, 15 Å/min), (e) 10 nm on sputtered HOPG (300 K, 15 Å/min), (f) 10 nm on SiO$_2$ (300 K, 15 Å/min). All spectra were recorded for various orientations of the incident electric field vector, $\vec{E}$, relative to the surface denoted by the blue, black and red curves, respectively, as depicted schematically in panel (b). Combining the analysis of the dichroism in the NEXAFS data and the XRD data allows a determination of the molecular orientation in the various films which is shown schematically in the insets of (c)–(f).

trast to our previous NEXAFS studies of pentacene films deposited on metals[15,30,31] or SiO$_2$ (Ref. 32) the corresponding analysis of aromatic molecules on graphite, however, is somewhat complicated by the overlapping C1s NEXAFS signatures of the molecular film and the substrate.

To begin with we discuss the undisturbed C1s NEXAFS spectra of pentacene. Figure 8(f) shows a set of spectra of a 10 nm pentacene film grown on SiO$_2$ which can be considered as a reference system of a film of uniformly oriented and weakly interacting molecules. Characteristic signatures in these spectra are distinct resonances at photon energies of 283–287 eV due to excitations of C1s electrons into closely spaced unoccupied π^* orbitals as well as broad resonances at higher energies which are attributed to excitations into σ^* orbitals. The theoretical analysis shows that the intensity of the π^* resonances depends on the orientation of the electrical field vector, $\vec{E}$, of the incident synchrotron light relative to the transition dipole moment, $\vec{T}$, which is oriented normal to

the ring plane of aromatic molecules [see Fig. 8(b)].[66] Thus, from NEXAFS measurements recorded for different angles of incidence of the incoming light, ε, the average tilt angle of $\vec{T}$ relative to the sample normal, α, can be determined. For substrates with threefold symmetry this yields the expression $I_{\pi^*} = \frac{1}{2}[P\cos^2\varepsilon(3\cos^2\alpha - 1) + 1 - \cos^2\alpha]$.[66,67] A quantitative analysis of the dichroism of the π^* resonances of the pentacene film on SiO_2 yields an angle of $\alpha = 79°$ which is in close agreement with XRD data showing an upright molecular orientation in the (001)-oriented films.

The C1s NEXAFS spectra of bare graphite [see Fig. 8(a)] exhibit two distinct peaks at photon energies of 285.4 and 291.7 eV which are assigned to π^* and σ^* resonances.[68] Hence, for pentacene covered HOPG a partial overlapping of the π^* regions occurs as shown exemplarily in Fig. 8(a) for a 5 nm film. To still extract a NEXAFS signature of the molecular film a substrate signal was subtracted from the measured spectrum before normalization in units of edge jump. To further account for the attenuation through the adlayer the substrate signal was accordingly weighted. This is possible because the distinct σ^* resonance of the substrate does not coincide with any pentacene related NEXAFS resonance which allows a scaling of the substrate spectrum so that no peak at 291.7 eV remains after subtraction of the substrate signal.

We note, that even after deposition of a nominal 20 nm pentacene film (data not shown) still a noticeable NEXAFS signature of the graphite substrate could be observed. Considering that the escape depth of electrons that are detected in the presently used partial electron yield only amounts to about 5.5 nm[69] this clearly indicates the formation of three-dimensional (3D) islands separated by deep crevices which is in line with the AFM data presented above [cf. Figs. 5(a) and 5(c)].

Figure 8(c) shows a set of NEXAFS spectra of a 1 nm pentacene film on HOPG which were recorded at different angles of incidence after subtraction of a graphite related background and subsequent normalization in units of the carbon edge jump. All spectra reveal at least 5 pronounced resonances in the π^* region at 283.7, 284.3, 284.6, 285.8, and 286.2 eV (indicated by dashed lines) and further peaks at 287.8, 288.9, 290.3, 293.8, and 300.4 eV which mainly can be attributed to σ^* resonances. The energetic positions of these resonances are virtually identical to those obtained for a thick film on SiO_2 [cf. Fig. 8(f)] but with a reversed dichroism. In particular we note, that no broadening of the π^* resonances occurs like in case of pentacene deposited on the coinage metals Cu, Ag, and Au (Refs. 15, 30, and 31) where a chemisorbed monolayer is formed. This is in agreement with the absence of any specifically bound monolayer on HOPG as inferred from our TDS data. The quantitative analysis of the dichroism yields an average tilt angle of the transition dipole moment (TDM) relative to the surface normal of $\alpha = 30° \pm 3°$ which reflects a rather recumbent orientation of the molecules as shown schematically in the inset in Fig. 8(c). Note, that this orientation compares well with the molecular arrangement adopted in the preferentially formed (022) plane of pentacene which yields an average tilt angle of the aromatic ring plane of 28° relative to the surface

plane. Moreover, keeping this crystallographic and molecular orientation in mind a nominal film thickness of 1 nm corresponds to about three molecular layers. Thus when considering planar adsorption geometry in the very first monolayer and a tilted assembly in the following two layers an average molecular tilt of about 18° would be expected. Since this value is clearly below the measured value it indicates that molecules in the bottom layer of such multilayer films are actually pitched and remain no-longer parallel to the HOPG surface. Because of the difficulties caused by the superposition of the intense substrate related NEXAFS signal the molecular orientation of (sub)monolayer pentacene films have not been determined by NEXAFS but a flat-lying adsorption geometry has been shown before.[47]

A very similar NEXAFS signature was observed for thicker films while the quantitative analysis of the dichroism yields a somewhat larger average tilt angle of up to 39° as shown in Fig. 8(d) for a 40 nm film. This angle can be related to the appearance of islands with other crystalline orientation which have been identified in the XRD measurements. In order to study furthermore the influence of growth parameters like temperature, rate and thickness on the resulting film structure additional films have been prepared at different substrate temperatures (230–350 K, including post deposition annealing at 385 K), different deposition rates (2–450 Å/min) and different thickness. Since the detailed analysis by means of XRD is rather time consuming (note, that a high-resolution $\theta/2\theta$ scan takes up to 12 h) the films have been characterized by NEXAFS. All these data (spectra not shown) are very similar to those displayed in Fig. 8(d) and the quantitative analysis yields tilt angles α in between 30° and 41° thus demonstrating that the film structure is robust and does not depend on growth parameters.

By contrast the substrate roughness, however, has a striking influence on the film structure and the molecular ordering. Figure 8(e) displays typical NEXAFS spectra of a film that was deposited onto a sputtered graphite sample to mimic a defective substrate surface. The absence of any dichroism in the NEXAFS data indicates either a complete disorder or an average tilt angle close to the magic angle of 55°. In view of the distinct diffraction pattern obtained in the corresponding XRD data an isotropic molecular orientation can be ruled out hence indicating an average orientation of $\alpha = 55°$ due to averaging over crystalline regions exhibiting different molecular orientations. Indeed a superposition of NEXAFS data where molecules are nearly upright [e.g., in Fig. 8(f)] and those of preferentially (022) oriented islands where pentacene molecules adopt a recumbent orientation [cf. Fig. 8(d)] yields nearly the same spectra as presented in Fig. 8(e).

F. Multilayer formation

While generally the low conductivity of molecular multilayer films hampers their characterization by means of STM and may cause artifacts such as unintentional removal of material[70] we have occasionally been able to image thin pentacene multilayer films. By using low tunneling currents of ≤ 30 pA pentacene islands with a thickness of up to 10 nm could be imaged with high resolution and without any
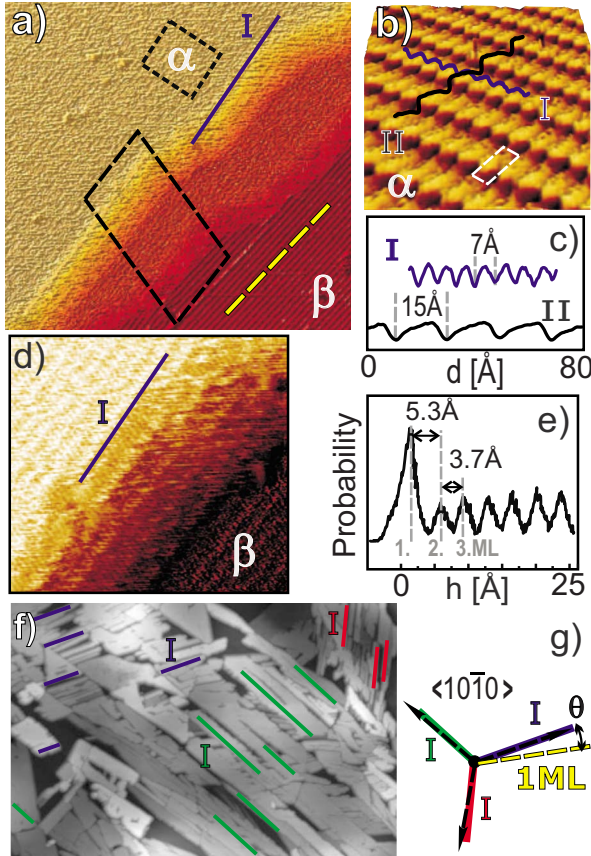
FIG. 9. (Color online) (a) Room-temperature STM micrograph showing the topography of a 6 nm pentacene island surrounded by a monolayer hemline (denoted as β). (b) High-resolution image of the topmost layer of the island [denoted as α in (a)] together with corresponding line scans (c). Panel (d) displays a high resolution image of the island edge showing the stacking of individual molecular layers and (e) the related height distribution. The AFM data (f) reveal a distinct azimuthal distribution of the individual islands which indicates an epitaxial orientation relative to the substrate (g).

noticeable damaging. This enabled us to derive important details on the initial stage of multilayer film growth which will be presented in the following.

After deposition of a pentacene film with a nominal thickness of 3 nm distinct and flat islands with heights up to 8 nm are formed. Figure 9(a) depicts an STM micrograph showing a partial view of one islands with an actual height of 6 nm surrounded by a monolayer hemline (denoted β) as evidenced by the characteristic row pattern (discussed before). In high resolution images it was possible to also resolve the molecular arrangement within the topmost layer of this island (denoted α) and to identify a rectangular unit cell with lateral dimensions of $d_I = 7 \pm 0.5$ Å and $d_{II} = 15 \pm 0.5$ Å [see line scans in Figs. 9(b) and 9(c)]. This unit cell compares well with the lateral periodicity of pentacene molecules in the (022) plane of the Siegrist phase yielding unit cell dimensions of 6.3 and 14.8 Å including an angle of 89.6°. The 3D STM-image of the monolayer indicates further a nonplanar orientation of the individual molecules which is in line with the arrangement of pentacene in (022) planes.

Another important piece of information was obtained from the height distribution of the individual molecular lay-

ers obtained in the high resolution STM data at the edge of the island [see in Figs. 9(d) and 9(e)]. To provide a more accurate calibration of the height scale than using the standard setting of the piezo scanner the (022) interlayer spacing ($d_{(022)}$=3.7 Å) deduced from the XRD measurements was used to crosscalibrate the apparent layer height in the STM data. Interestingly, this yields a distinctly larger separation between the first and second monolayer of 5.3 Å and thus indicates a modified stacking at the bottom of multilayers which will be discussed in detail in the next section.

Like in case of the monolayer also the multilayer islands of pentacene are found to be locally (i.e., on single grains of graphite) not isotropically distributed but instead reveal three distinct azimuthal orientations. This is evident when plotting the azimuthal distribution of the long sides of the elongated islands [indicated by solid lines in Fig. 9(f)]. STM data of thin multilayer islands displayed in Fig. 9(a) reveal a pattern of small depressions at the topmost layer (line I) that can be associated with the head-to-head boundaries [line in Fig. 9(b)]. These lines appear at an angle of about 10° relative to the characteristic rows of the monolayer (dashed line) which themselves are rotated by $\pm 10°$ with respect to the $\langle 10\bar{1}0 \rangle$ direction of the substrate. Thus, the long island axes appear also to be epitaxially aligned along these substrate azimuth directions as indicated in Fig. 9(g).

IV. DISCUSSION

We begin our discussion with the interaction strength of pentacene molecules with the graphite substrate. Thermal desorption spectra which were recorded for pentacene films of various thicknesses yielded only a multilayer desorption peak while no evidence for any additional desorption signal due to a more firmly bound monolayer was found like for the case of pentacene adsorbed on the coinage metals Cu, Ag, and Au.[15,31,32] Interestingly, even the thermal desorption signal of submonolayer films can be well described by a zero order kinetics which reflects the formation of multilayer islands upon heating before they desorb. This indicates that pentacene molecules are actually less strongly bound to the graphite surface than in the pentacene crystal. An estimate of the molecular adsorption energy can be made on the basis of effective pair potential energies which have been derived previously from a systematic analysis of TDS data recorded for various PAHs on HOPG.[52,71] Using the derived values of the interaction energies (H-HOPG: 27 meV, C-HOPG: 52 meV) this yields an adsorption energy for pentacene on graphite of 1.14 eV which is distinctly lower than the pentacene sublimation enthalpy of 1.63 eV (156.9 kJ/mol).[57] Such a rather weak substrate interaction is also evidenced by the similarity of the reorganization energy of pentacene in the gas phase (108 meV)[72] and on graphite (118 meV)[51,73] derived from ultraviolet photoemission spectroscopy (UPS) measurements. In contrast, for a chemisorbed monolayer on Au(111) a distinctly larger value of 174 meV has been observed.[74] The absence of any additional electronic interaction between the pentacene molecules and the substrate is further corroborated by the fact that no differences in the NEXAFS signature of 1 nm and multilayer films were ob-

served. By contrast, for pentacene monolayers chemisorbed on metals a distinct broadening of the π^* subresonances was found in the C1s NEXAFS data together with the appearance of an additional desorption peak at significantly higher temperatures than the multilayer desorption.[15,30,31] In particular the present result demonstrates the failure of the preparation of a distinct pentacene monolayer on graphite by selective desorption of multilayer excess which has been reported previously.[50] We note further, that previous DFT calculations also found a stronger electronic interaction of pentacene with graphite than with neighboring molecules (40 vs 11 meV),[75] which is not consistent with the present data and can be attributed to the well-known difficulty of DFT calculations to properly describe van der Waals interactions.

In the (sub)monolayer regime pentacene forms well-ordered islands on graphite where molecules exhibit a planar adsorption geometry with their ring plane oriented parallel to the surface plane and adopt a $\left(\begin{smallmatrix} 7 & 0 \\ -1 & 3 \end{smallmatrix} \right)$ superstructure. According to the symmetry of the substrate these structures appear in six rotational and mirror domains. Note that by carefully analyzing the relative orientation of all domains as well as their registry with respect to the substrate lattice the structure could be identified rather precisely. The unit cell area of the structure amounts to 110.1 Å^2 which is somewhat larger than the van der Waals box dimensions of the molecular plane of pentacene (99.8 Å^2). This shows that in the monolayer the molecules are not densely packed which is caused by their epitaxial registry on the graphite lattice and leads to the formation of a characteristic row pattern which can be observed in the STM data. In a previous low temperature STM study Chen *et al.* also have investigated the adsorption of pentacene on HOPG and observed a similar molecular arrangement for the monolayer but reported somewhat different unit cell parameters yielding an area per molecule of 125.6 Å^2.[49] We note, however, that in contrast to our intrinsic calibration by also imaging the bare graphite lattice the authors relied on the standard piezo calibration which only provides a limited accuracy.[76]

Upon further deposition multilayer films are formed which are composed of islands with lateral extensions of several micrometers and ultra-flat surfaces exhibiting monomolecular steps (cf. Fig. 5). X-ray diffraction data show further that such molecular layers are well-ordered and crystallize in the Siegrist bulk-phase forming preferentially (022)-oriented films while for thick films (>100 nm) also some other crystalline orientations have been identified. In all these crystalline planes pentacene molecules are slightly tilted (about 28°−32°) around their long axis but still reveal a recumbent orientation with respect to the substrate surface. Qualitatively such a molecular orientation has been deduced previously from UPS data[77] while no precise angles were derived. The resulting molecular and crystalline orientation of such films thus bear close resemblance to those formed upon pentacene deposition onto Au(111) or Ag(111).[30,31] A striking difference, however, is the absence of a pronounced dewetting which leads on metals to the formation of tall organic islands with a small base area hence raising the question about the origin for the rather different morphology of pentacene films on HOPG and metals.

The key to understand the underlying mechanism yields a closer inspection of the initial stage of multilayer formation.
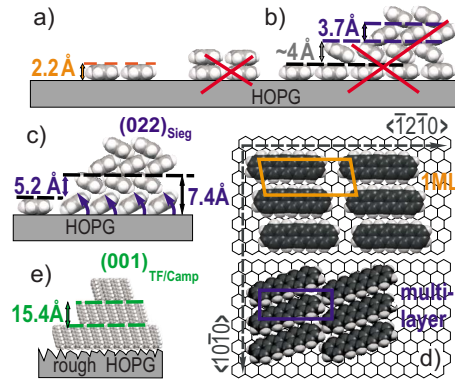

FIG. 10. (Color online) Summary of possible film structures adopted upon pentacene film growth on graphite: (a) first monolayer, (b) hypothetic multilayer structures including a planar stacking and formation of (022)-oriented films on a nonrelaxed, and (c) a relaxed first monolayer. The lateral superstructure of monolayers and multilayers formed on perfect HOPG are compared in (d), and the resulting growth on a rough HOPG substrate is shown in panel (e).

By combining STM, XRD, and NEXAFS data we are able to demonstrate that the undermost layer of the multilayer films is actually lifted. At (sub)monolayer coverage the molecules adsorb flat-lying on the graphite substrate yielding an effective layer height of 2.2 Å [cf. Fig. 2(c)] which is in close agreement with the van der Waals thickness of about 2.4 Å. With increasing film thickness this molecular orientation is, however, not maintained and instead (022)-oriented crystalline islands are formed where molecules are slightly tilted and adopt an interlayer spacing of $d_{(022)}=3.7$ Å. By using this interlayer spacing derived from XRD data to crosscalibrate the height distribution of the STM data we could rather precisely measure the step height between the first monolayer in the hemline around a pentacene island and the second monolayer within the island which yields a value of 5.3 Å [see Fig. 9(e)]. Comparing this value with the possible packing motifs in a molecular island [cf. Figs. 10(b) and 10(c)] indicates that actually the bottommost layer of the island is also tilted. This yields an expected step of 2 × 3.7 Å−2.2 Å=5.2 Å which is in excellent agreement with the measured step height. Such a lifting is further corroborated by the average tilt angle derived from NEXAFS measurements for thin multilayer films. Note, that the lateral molecular packing density within the (022) plane is distinctly larger than for the pentacene monolayer and yields a molecular area of 93.2 Å^2 which can only be realized by tilting of the molecules.

Interestingly, the (022)-oriented pentacene islands are not azimuthally isotropic distributed but reveal a distinct orientational ordering with respect to the graphite lattice. The detailed analysis yields an epitaxial orientation of the molecular head sides along the $\langle 10\bar{1}0 \rangle$ azimuth of the substrate [cf. Fig. 10(d)] and can formally be described as a $\left(\begin{smallmatrix} 6 & 0 \\ -1.5 & 3 \end{smallmatrix} \right)$ superstructure. Apparently this film structure is stabilized by higher-order commensurability with respect to the substrate. Comparing the lateral molecular packing density in the (022) plane and the pentacene monolayer reveals an increase of

about 33% when going to the multilayer films. Thus, when considering a conservation of mass a lateral compression upon multilayer formation may be expected which is in line with the development of individual islands separated by deep crevices. We note that the epitaxial growth proceeds only on a local scale at dimensions of individual graphite grains while on a macroscopic scale the film orientation is limited by the azimuthally isotropic distribution of graphite grains of HOPG [cf. Fig. 5(e)]. Therefore the previously reported epitaxial growth of (001)-oriented anthracene crystallites on HOPG appears to be rather fortuitous[45] especially since the molecules in such crystallites are upright oriented and reveal no epitaxial relation with the underlying graphite lattice.

The present analysis thus highlights the importance of some flexibility to (slightly) reorient the prealigned molecules at the interface in order to reduce the strain due to a misfit between the molecular ordering in the seed monolayer and in crystalline multilayers. A similar molecular tilting has been observed for tetracene molecules on Ag(111) upon completion of the first monolayer.[78] In contrast, for the next larger acene the adsorption energy on silver becomes so large that a lifting of pentacene molecules at the interface is not possible and they remain flat lying in the first monolayer and cause a pronounced islanding upon further growth.[31] This accentuates further the relevance of the balance between adsorption energy at the substrate and sublimation energy of the molecular material.

Furthermore, it was found that the resulting pentacene film structure (molecular orientation as well as crystalline phase) also depends sensitively on the substrate roughness. At regions where the HOPG surface has defects (i.e., imperfect cleavage or grain boundaries) or exhibits a microscopic roughness pentacene molecules grow in an upright orientation. This aspect has been carefully verified by growing additional pentacene films onto intentionally roughened graphite surfaces which were sputtered after exfoliation. Corresponding x-ray diffraction data [cf. Fig. 7(c)] showed further that on such rough HOPG surfaces pentacene forms (001)-oriented films which adopt initially the so-called *thin film* crystal phase while they continue to grow in the Campbell bulk phase with increasing film thickness. This growth scenario thus parallels the situation observed before for pentacene film growth on several other noninteracting or weakly interacting substrates like SiO_2,[20,23] Al_2O_3,[79] or on self-assembled monolayers of thiols[30] or silanes.[65] Here, the intermolecular interaction between pentacene dominates the substrate-monolayer interaction which favors the formation of thermodynamically most stable (001)-oriented films.[64]

Since the adsorption energy of pentacene on graphite is also lower than the molecular bulk sublimation enthalpy but notwithstanding yields the formation of (022)-oriented films this points toward another important aspect. In contrast to the before mentioned inert substrates the graphite basal plane allows the formation of an epitaxially ordered monolayer which apparently provides sufficient stabilization to prevent a spontaneous up standing of molecules in the very first monolayer. Such an additional stabilization is absent on mi-

croscopically rough graphite surfaces where in fact molecules grow in an upright orientation, further stressing the relevance of coherent ordering at the substrate surface to enable a template effect.

Finally we note, that upright oriented pentacene molecules were also observed in previous studies by Chen *et al.* and by Parisse *et al.* for multilayer films on HOPG.[49,80] Based on our detailed growth study we conclude, however, that this structural motif is not representative for pentacene on HOPG, but rather marks an exception appearing only at defective or rough graphite substrates. Hence follows the importance of using complementary analysis techniques to derive a complete picture of organic films growth instead of only using a local microscopy technique.

V. CONCLUSIONS

The evolution and microstructure of pentacene films on HOPG have been analyzed and an epitaxial growth of (022)-oriented films is demonstrated where molecules adopt a recumbent orientation. Based on our microscopic structural analysis we were able to identify some important key factors which enable this particular film growth. Molecules initially adsorb prealigned with their ring plane parallel to the surface and form a (locally) commensurate but not densely packed monolayer which is stabilized by the close match of the carbon frame of the molecules and the substrate. A further condition is the rather weak adsorption energy of the molecules on graphite which enables a slight tilting of the molecules at the interface and thus allows the formation of crystalline multilayer films by suppressing any strain due to lattice mismatch between the molecular film and the substrate. Most likely this small activation of the molecular tilting is compensated by the gain in lattice energy due to the closer packing achieved in the (022) planes which further became energetically stabilized by the epitaxial relation with respect to the basal plane of graphite. In contrast, on metal surfaces molecules are chemisorbed and form a dense-packed seed layer which usually hampers an adaptation to the molecular lattice and results in a large lattice mismatch and pronounced islanding. Moreover, it is shown that the resulting film structure changes drastically if the graphite surface exhibits defects or becomes rough so that no (locally) ordered monolayer film can be formed and the template effect due to prealigned molecules is no longer operative. In that case molecules adsorb in an upright orientation and continue to grow as (001)-oriented films thus showing the importance to avoid surface roughness when utilizing template-guided molecular film growth.

*gregor.witte@physik.uni-marburg.de

[1] Y. Shirota, J. Mater. Chem. **10**, 1 (2000).

[2] C. D. Dimitrakopoulos and P. R. L. Malenfant, Adv. Mater. **14**, 99 (2002).

[3] S. R. Forrest, Nature (London) **428**, 911 (2004).

[4] G. Hadziioannou and G. G. Malliaras, *Semiconducting Polymers* (Wiley-VCH, New York, 2007), Vol. 1.

[5] Z. Bao and J. Locklin, *Organic Field-Effect Transistors* (CRC Press, Boca Raton, 2007).

[6] G. Witte and Ch. Wöll, J. Mater. Res. **19**, 1889 (2004).

[7] F. Schreiber, Phys. Status Solidi A **201**, 1037 (2004).

[8] T. Siegrist, C. Kloc, J. H. Schön, B. Batlogg, R. C. Haddon, S. Berg, and G. A. Thomas, Angew. Chem. Int. Ed. **40**, 1732 (2001).

[9] N. Karl, *Organic Electronic Materials*, edited by R. Farchioni and G. Grosso (Springer, Berlin, 2001).

[10] J. Cornil, J. P. Calbert, and J. L. Bredas, J. Am. Chem. Soc. **123**, 1250 (2001).

[11] A. Andreev, G. Matt, C. J. Brabec, H. Sitter, D. Badt, H. Sey-ringer, and N. S. Sariciftci, Adv. Mater. **9**, 12 (2000).

[12] P. Ruffieux, O. Gröning, M. Bielmann, C. Simpson, K. Müllen, L. Schlapbach, and P. Gröning, Phys. Rev. B **66**, 073409 (2002).

[13] A. Hoshino, Y. Takenaka, and H. Miyaji, Acta Crystallogr., Sect. B: Struct. Sci. **59**, 393 (2003).

[14] C. Menozzi, V. Corradini, M. Cavallini, F. Biscarini, M. G. Betti, and C. Mariani, Thin Solid Films **428**, 227 (2003).

[15] S. Söhnchen, S. Lukas, and G. Witte, J. Chem. Phys. **121**, 525 (2004).

[16] P. Guaino, D. Carty, G. Hughes, O. McDonald, and A. A. Cafolla, Appl. Phys. Lett. **85**, 2777 (2004).

[17] D. J. Gundlach, Y. Y. Lin, T. N. Jackson, S. F. Nelson, and D. G. Schlom, IEEE Electron Device Lett. **18**, 87 (1997).

[18] H. Klauk, M. Halik, G. Zschieschang, G. Schmidt, W. Radik, and W. Weber, J. Appl. Phys. **92**, 5259 (2002).

[19] R. Ruiz, D. Choudhary, B. Nickel, T. Toccoli, K.-C. Chang, A. C. Mayer, P. Clancy, J. M. Blakely, R. L. Headrick, S. Iannotta, and G. G. Malliaras, Chem. Mater. **16**, 4497 (2004).

[20] I. P. M. Bouchoms, W. A. Schoonveld, J. Vrijmoeth, and T. M. Klapwijk, Synth. Met. **104**, 175 (1999).

[21] M. Brinkmann, S. Graff, C. Straupe, J.-C. Wittmann, C. Chaumont, F. Nuesch, A. Aziz, M. Schaer, and L. Zuppiroli, J. Phys. Chem. B **107**, 10531 (2003).

[22] T. Minakata, H. Imai, M. Ozaki, and K. Saco, J. Appl. Phys. **72**, 5220 (1992).

[23] C. D. Dimitrakopoulos, A. R. Brown, and A. Pomp, J. Appl. Phys. **80**, 2501 (1996).

[24] S. Verlaak, S. Steudel, P. Heremans, D. Janssen, and M. S. Deleuze, Phys. Rev. B **68**, 195409 (2003).

[25] B. Stadlober, U. Haas, H. Maresch, and A. Haase, Phys. Rev. B **74**, 165302 (2006).

[26] T. Kakudate, N. Yoshimoto, K. Kawamura, and Y. Saito, J. Cryst. Growth **306**, 27 (2007).

[27] G. E. Thayer, J. T. Sadowski, F. Meyer zu Heringdorf, T. Sakurai, and R. M. Tromp, Phys. Rev. Lett. **95**, 256106 (2005).

[28] A. Al-Mahboob, J. T. Sadowski, T. Nishihara, Y. Fujikawa, Q. K. Xue, K. Nakajima, and T. Sakurai, Surf. Sci. **601**, 1304 (2007).

[29] C. B. France, P. G. Schroeder, J. C. Forsythe, and B. A. Parkinson, Langmuir **19**, 1274 (2003).

[30] D. Käfer, L. Ruppel, and G. Witte, Phys. Rev. B **75**, 085309 (2007).

[31] D. Käfer and G. Witte, Chem. Phys. Lett. **442**, 376 (2007).

[32] D. Käfer, C. Wöll, and G. Witte, Appl. Phys. A: Mater. Sci. Process. **95**, 273 (2009).

[33] A. K. Geim and K. S. Novoselov, Nature Mater. **6**, 183 (2007).

[34] T. O. Wehling, K. S. Novoselov, S. V. Morozov, E. E. Vdovin, M. I. Katsnelson, A. K. Geim, and A. I. Lichtenstein, Nano Lett. **8**, 173 (2008).

[35] B. Sanyal, O. Eriksson, U. Jansson, and H. Grennberg, Phys. Rev. B **79**, 113409 (2009).

[36] U. Bardi, S. Magnanelli, and G. Rovida, Langmuir **3**, 159 (1987).

[37] U. Zimmermann and N. Karl, Surf. Sci. **268**, 296 (1992).

[38] C. Ludwig, B. Gompf, W. Glatz, J. Petersen, W. Eisenmenger, M. Möbus, U. Zimmermann, and N. Karl, Z. Phys. B: Condens. Matter **86**, 397 (1992).

[39] A. Stabel and J. P. Rabe, Synth. Met. **67**, 47 (1994).

[40] A. Stabel, P. Herwig, K. Müllen, and J. P. Rabe, Angew. Chem. Int. Ed. Engl. **34**, 1609 (1995).

[41] R. Strohmaier, J. Petersen, B. Gompf, and W. Eisenmenger, Surf. Sci. **418**, 91 (1998).

[42] K. Walzer, M. Sternberg, and M. Hietschold, Surf. Sci. **415**, 376 (1998).

[43] X. Qiu, Ch. Wang, Q. Zeng, B. Xu, S. Yin, H. Wang, S. Xu, and C. Bai, J. Am. Chem. Soc. **122**, 5550 (2000).

[44] G. M. Flori, T. L. Werblowski, T. Müller, B. J. Berne, and G. W. Flynn, J. Phys. Chem. B. **109**, 4520 (2005).

[45] S. Jo, H. Yoshikawa, A. Fujii, and M. Takenaga, Surf. Sci. **592**, 37 (2005).

[46] B. Jaeckel, J. Sambur, and B. A. Parkinson, J. Phys. Chem. C **113**, 1837 (2009).

[47] Y. Harada, H. Ozaki, and K. Ohno, Phys. Rev. Lett. **52**, 2269 (1984).

[48] N. Koch, A. Vollmer, I. Salzmann, B. Nickel, H. Weiss, and J. P. Rabe, Phys. Rev. Lett. **96**, 156803 (2006).

[49] W. Chen, H. Huang, A. Thye, and S. Wee, Chem. Commun. (Cambridge) **36**, 4276 (2008).

[50] M. Shionoiri, M. Kozasa, S. Kera, K. K. Okudaira, and N. Ueno, Jpn. J. Appl. Phys. **46**, 1625 (2007).

[51] H. Yamane, S. Nagamatsu, H. Fukagawa, S. Kera, R. Friedlein, K. K. Okudaira, and N. Ueno, Phys. Rev. B **72**, 153412 (2005).

[52] R. Zacharia, H. Ulbricht, and T. Hertel, Phys. Rev. B **69**, 155406 (2004).

[53] F. Ortmann, W. G. Schmidt, and F. Bechstedt, Phys. Rev. Lett. **95**, 186101 (2005).

[54] A. Schöll, Y. Zou, T. Schmidt, R. Fink, and E. Umbach, J. Electrost. **129**, (Spec.), 1 (2003).

[55] B. Watts, L. Thomsen, and P. C. Dastoor, J. Electrost. **151**, 105 (2006).

[56] E. Habenschaden and J. Küppers, Surf. Sci. **138**, L147 (1984).

[57] V. Oja and E. M. Suuberg, J. Chem. Eng. Data **43**, 486 (1998).

[58] H. Ozaki, J. Chem. Phys. **113**, 6361 (2000).

[59] N. Ferralis, K. Pussi, S. E. Finberg, J. Smerdon, M. Lindroos, R. McGrath, and R. D. Diehl, Phys. Rev. B **70**, 245407 (2004).

[60] The XRD powder spectra were calculated using the visualization and analysis program (Mercury) of the Cambridge crystal strucural databes (CCSD) software package.

[61] R. B. Campbell, J. M. Robertson, and J. Trotter, Acta Crystallogr. **15**, 289 (1962).

[62] H. Yoshida, K. Inaba, and N. Sato, Appl. Phys. Lett. **90**, 181930

(2007).

[63] S. Schiefer, M. Huth, A. Dobrinevski, and B. Nickel, J. Am. Chem. Soc. **129**, 10316 (2007).

[64] D. Choudhary, P. Clancy, R. Shetty, and F. Escobedo, Adv. Funct. Mater. **16**, 1768 (2006).

[65] D. Knipp, R. A. Street, A. Völkel, and J. Ho, J. Appl. Phys. **93**, 347 (2003).

[66] J. Stöhr, *NEXAFS Spectroscopy*, Springer Series in Surface Science (Springer, New York, 1992), Vol. 25.

[67] J. Stöhr and D. A. Outka, Phys. Rev. B **36**, 7891 (1987).

[68] R. A. Rosenberg, P. J. Love, and V. Rehn, Phys. Rev. B **33**, 4034 (1986).

[69] D. Käfer, L. Ruppel, G. Witte, and Ch. Wöll, Phys. Rev. Lett. **95**, 166602 (2005).

[70] G. Witte and Ch. Wöll, Phys. Status Solidi A **205**, 497 (2008)

[71] H. Ulbricht, R. Zacharia, N. Cindir, and T. Hertel, Carbon **44**, 2931 (2006).

[72] V. Coropceanu, M. Malagoli, D. A. da Silva Filho, N. E. Gruhn, T. G. Bill, and J. L. Bredas, Phys. Rev. Lett. **89**, 275503 (2002).

[73] N. Ueno, S. Kera, K. Sakamoto, and K. K. Okudaira, Appl. Phys. A: Mater. Sci. Process. **92**, 495 (2008).

[74] N. Koch, A. Vollmer, S. Duhm, Y. Sakamoto, and T. Suzuki, Adv. Mater. **19**, 112 (2007).

[75] P. B. Paramonov, V. Coropceanu, and J.-L. Bredas, Phys. Rev. B **78**, 041403(R) (2008).

[76] We note further that the angle among the unit cell vectors reported by Chen *et al.* (Ref. 49) does not agree with the STM data displayed in Ref. 49 thus indicating some problems with the calibration.

[77] H. Fukagawa, H. Yamane, T. Kataoka, S. Kera, M. Nakamura, K. Kudo, and N. Ueno, Phys. Rev. B **73**, 245310 (2006).

[78] A. Langner, A. Hauschild, S. Fahrenhoz, and M. Sokolowski, Surf. Sci. **574**, 153 (2005).

[79] A.-L. Deman, M. Eroul, D. Lallemann, M. Phaner-Goutorbe, P. Lang, and J. Tardy, J. Non-Cryst. Solids **354**, 1598 (2008).

[80] P. Parisse, S. Picozzi, M. Passacantando, and L. Ottaviano, Thin Solid Films **515**, 8316 (2007).